Formation of Nanocrystalline Structures by Crystallization of Amorphous Fe-M-B (M=IVa to VIa Group Metal) Alloys

Sci. Rep. RITU A39 (1994) pp. 133-140
No. 2, January 1994

Formation of Nanocrystalline Structures by Crystallization of Amorphous Fe-M-B (*M*=IVa to VIa Group Metal) Alloys*

Kiyonori Suzuki, Akihiro Makino, Akihisa Inoue[1] and Tsuyoshi Masumoto[1]
Central Research Laboratory, Alps Electric Co., Ltd., Nagaoka 940 Japan.
[1]*Institute for Materials Research, Tohoku University, Sendai 980 Japan.*

(Received January 7,1994)

The formation range, crystallization behavior, annealing-induced phase and its magnetic properties were investigated for amorphous $Fe_{93-x}M_7B_x$ (*M*=Ti, Zr, Hf, V, Nb, Ta, Cr, Mo and W) alloys. It was found that the crystallization process of the amorphous Fe-M-B alloys can be classified into two types where the primary precipitates are a bcc single phase (*M*=Zr, Hf, V, Nb, Cr and Mo) or coexistent bcc and tetragonal-Fe_3B phases (*M*=Ti, Ta and W). The grain size of the primary crystallized Fe-M-B alloys was evaluated to be 10 to 20 nm for *M*=Ti, Zr, Hf, Nb, Ta and W, being smaller than those (30 to 50 nm) for *M*=V, Cr and Mo. The small grain size of the alloys containing the former *M* elements seems to reflect the small growth rate of the primary precipitates resulting from the large re-distribution of the *M* elements between the primary bcc and residual amorphous phases which is due to their small solubility to α-Fe as well as their small diffusivity. The volume density of primary bcc precipitates showed the tendency to increase with increasing heating rate. This microstructural change results in a significant increase of the permeability (μ_e) of the nanocrystalline alloys and high μ_e values of 24000-38000 at 1 kHz and 0.4 A/m are obtained for the Fe-M-B (*M*=Zr, Hf and Nb) alloys annealed with a heating rate of 3.3 K/s.

KEYWORDS: nanocrystalline alloys, crystallization, soft magnetic properties, amorphous alloys

1. Introduction

Recently, it has been reported that nanocrystalline alloys obtained by crystallization of melt-spun amorphous alloys exhibit excellent soft magnetic properties. Typical nanocrystalline soft magnetic alloys have been found in Fe-Si-B-Nb-Cu[1], Fe-M-B (*M*=Zr and Hf)[2] and Fe-P-C-Cu-Ge[3] systems. Soft magnetic properties of nanocrystalline materials have been explained[4] on the basis of the random anisotropy model and are strongly dependent on grain size and grain boundary structure. Among these nanocrystalline alloys, the highest Fe concentration, which results in the highest saturation magnetization (1.7T), has been achieved in the Fe-Zr-B system because of the high glass-forming ability of Zr for Fe and the formation of the nanocrystalline-bcc phase without the addition of non-magnetic elements such as Cu, Nb and Ge. We have further found[5] the formation of a similar nanocrystalline-bcc phase in an Fe-Nb-B ternary system.

The formation of nano-structure in the Fe-Si-B-Nb-Cu system has been studied[6, 7] in detail and been explained by the combination of an accelerated nucleation rate resulting from the immiscibility of Cu to Fe and a reduced crystal growth rate due to the small diffusivity of Nb. However, little has been known about the reason for the formation of the nanocrystalline structure in such a simple Fe-M-B system. In addition, there is a possibility that a similar nanocrystalline structure forms by the replacement of Zr, Hf and Nb by other transition elements. This paper is intended to examine the possibility for the formation of nanocrystalline-bcc structure in an annealed state of amorphous Fe-M-B (*M*=transition metal) alloys and to investigate the dominant factors for the formation of the nanocrystalline-bcc phase.

2. Experimental Procedure

Fe-B binary, Fe-M-B (*M*=Ti, Zr, Hf, V, Nb, Ta, Cr, Mo and W) ternary alloy ingots were prepared by arc melting mixtures of a pre-alloyed Fe-B (8.9 mass%B) alloy and pure Fe, and *M* metals in an argon atmosphere. From the master alloy ingots, rapidly solidified ribbons with cross sections of about 1 x 0.02 and 14 x 0.02 mm^2 were produced in an argon atmosphere by the single roller melt-spinning technique. The compositions are nominally expressed in atomic per cent. The rapidly solidified sample was heated up to various temperatures with a differential thermal analysis (DTA) apparatus at a constant heating rate of 0.17 K/s under an argon atmosphere. Structures of rapidly solidified and heated samples were examined by x-ray diffractometry using Co-Kα radiation and transmission electron microscopy (TEM). A Perrkin-Elmer DSC-7 was used for isothermal differential scanning calorimetry (DSC) experiments. The lattice spacing (d_{110}) was evaluated from the $(110)_{bcc}$ reflection peak measured by the step scanning method. The diffraction angle was calibrated on the basis of the reflection angle of the internal standard material (pure Si powder, *640a*). The mean grain size (*D*) was evaluated by using Scherrer's equation from the half-width of $(110)_{bcc}$ reflection peak. The broadening of diffraction

* IMR, Report No.1955

line due to the width of x-ray source was removed by Warren's method[8]. Relative permeability (μ_e) was measured with straight-strip (1 mm in width and 60 mm in length) and ring (6 mm in inner- and 10 mm in outer-diameter) shaped samples by a vector impedance analyzer.

3. Results

3. 1. *Glass formation range in Fe-M-B ternary alloys*

Figures 1(a), 1(b) and 1(c) show the compositional dependence of the μ_e value for the Fe-Zr-B[2], Fe-Hf-B[9] and Fe-Nb-B[5] ternary alloys, respectively, obtained by annealing

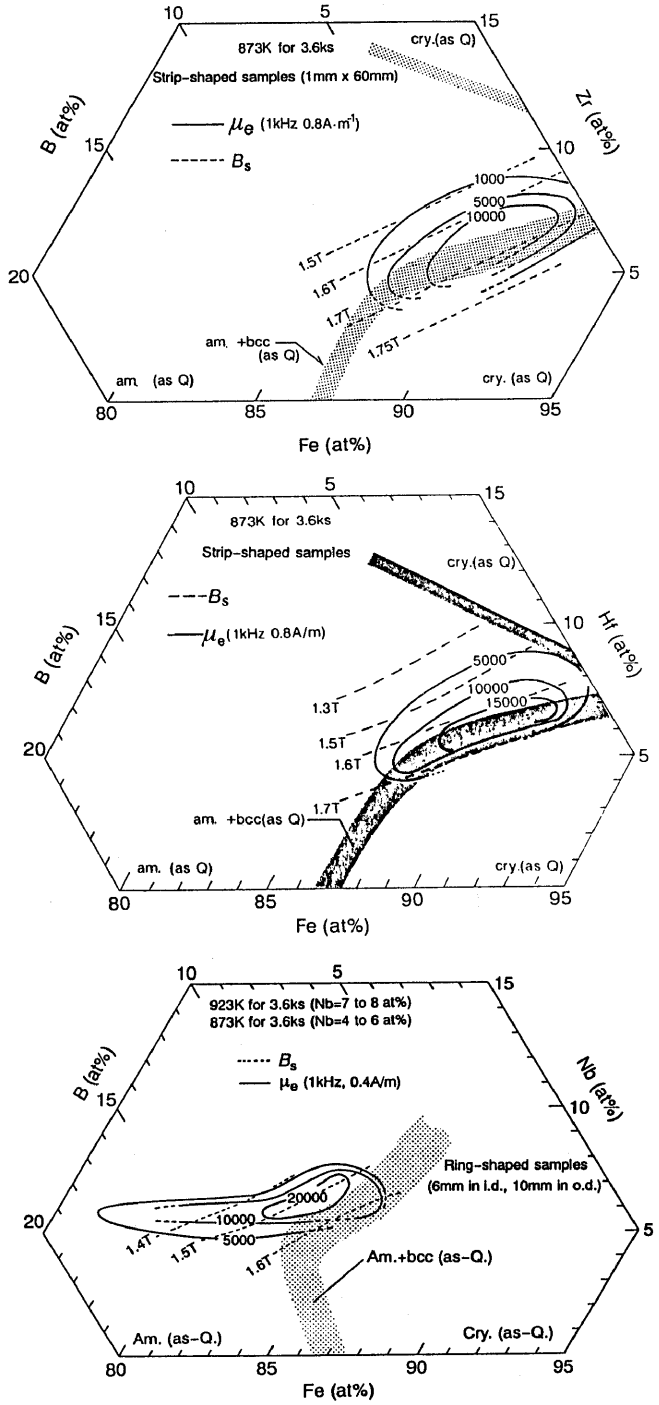

Fig. 1 Compositional dependence of μ_e and B_s for melt-spun Fe-Zr-B[2] (a), Fe-Hf-B[9] (b) and Fe-Nb-B[5] (c) alloys annealed for 3.6 ks at 873 K or 923 K. The data of the phase field in a rapidly solidified state are also shown for reference.

of the rapidly solidified phase for 3.6 ks at 873 or 923 K. In these Fe-M-B ternary systems, the nanocrystalline bcc phase with grain sizes <20 nm has been confirmed to form in the range of 5 to 7 %Zr and 1 to 8 %B for M=Zr, 5 to 9 %Hf and 1 to 8 %B for M=Hf and 5 to 7 %Nb and 8 to 15%B for M=Nb. The deviation of M and B content from these composition ranges causes the degradation of soft magnetic properties because of the precipitation of compounds or an increase of the grain size. The alloy compositions of $Fe_{93-x}M_7B_x$ (M=IVa to VIa group transition metal) were therefore chosen in the subsequent study for the purpose of examining the possibility for formation of the nanocrystalline bcc structure.

Figure 2 shows the glass formation ranges in the $Fe_{93-x}M_7B_x$ alloys, along with that for Fe-B binary alloys. The phase field shown in Fig. 2 was determined by x-ray diffraction analysis. No significant difference in glass formation range is seen for M=V and Cr, in comparison with that for the Fe-B binary system. However, the minimum B content for the formation of an amorphous single phase in Fe-B alloys decreases by the addition of the other M elements, and tends to increase with an increase of the group number of M elements. This tendency is thought to reflect the glass forming ability of M elements for the Fe-M-B system. That is, the effectiveness of M metals for the formation of an amorphous phase is the greatest for Zr and Hf and decreases in the order of Nb > Ti=Ta > Mo=W > V=Cr. The nanocrystalline bcc structure was found to form in the low B content region where the bcc phase precipitates as a primary phase in the decomposition process of the amorphous phase. Thus, the most intensive tendency for formation of the bcc phase

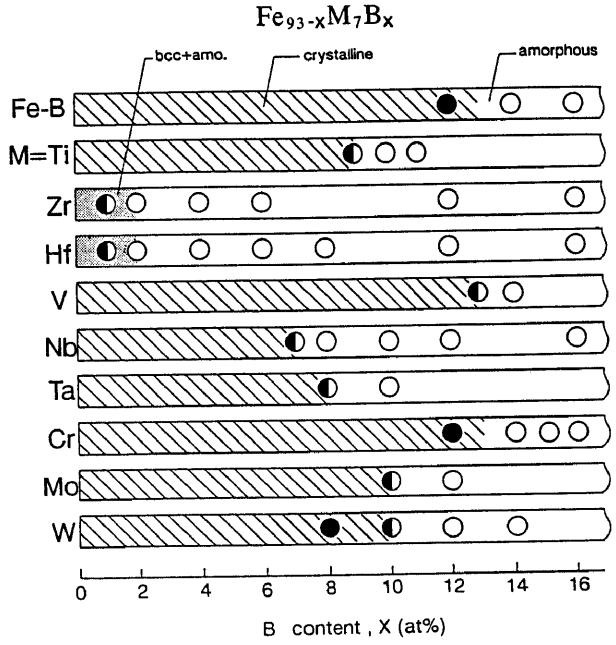

Fig. 2 Change in the phase field as a function of B content for melt-spun $Fe_{93-x}M_7B_x$ (M=Ti, Zr, Hf, V, Nb, Ta, Cr, Mo and W) ternary alloys. The data of Fe-B binary alloys are also shown for comparison.

should be predictable at the compositions with the minimum B content in each amorphous Fe-7%M-B ternary alloy.

3. 2. *Formation of nanocrystalline structures in Fe-M-B ternary alloys*

Figure 3 shows the DTA curves of amorphous $Fe_{93-x}M_7B_x$ ternary alloys with the minimum B content for the formation of an amorphous phase in each system. The DTA curve of an amorphous $Fe_{86}B_{14}$ alloy is also shown for comparison. Two or more than three exothermic peaks are seen on all the DTA curves of the amorphous $Fe_{93-x}M_7B_x$ ternary alloys, indicating that these amorphous alloys crystallize through multi stages. In order to examine the structural change at the first exothermic peak in each DTA curve, x-ray diffractometry analysis was made for the samples heated up to the temperature (T_f) between the first and the second exothermic peaks in each DTA curve. As shown in Fig. 4, only a $(110)_{bcc}$ reflection peak is seen in the diffraction patterns of the Fe-7%M-B (M=Zr, Hf, V, Nb, Cr and Mo) alloys, revealing that the first exothermic peak for these alloys is due to the structural change from amorphous to bcc phase. On the contrary, reflection lines from the mixed structure consisting of bcc and tetragonal-Fe_3B are seen in the diffraction patterns of the Fe-7%M-B (M=Ti, Ta and W) samples heated up to the temperature just above the first exothermic peak, indicating that the simultaneous precipitation of bcc and compound phases takes place at the first stage of crystallization. The reaction at the first stage crystallization of amorphous $Fe_{86}B_{14}$ alloy is well known as a typical example of primary crystallization[10], that is, the reaction is due to the structural change from an amorphous to a mixed structure

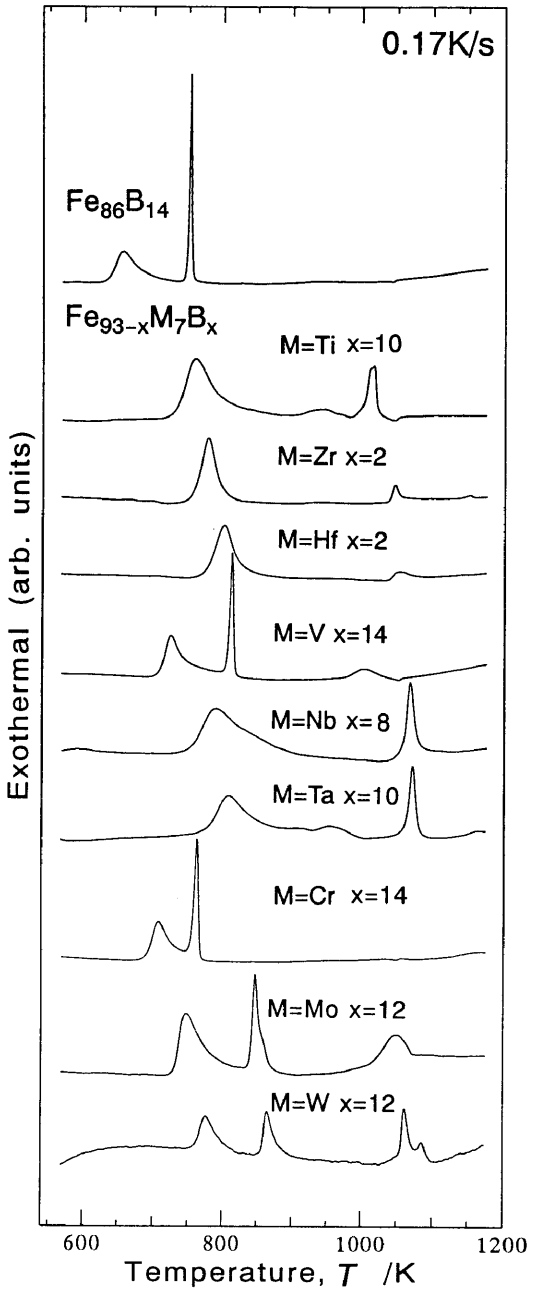

Fig. 3 DTA curves of amorphous $Fe_{93-x}M_7B_x$ (M=Ti, Zr, Hf, V, Nb, Ta, Cr, Mo and W) alloys.

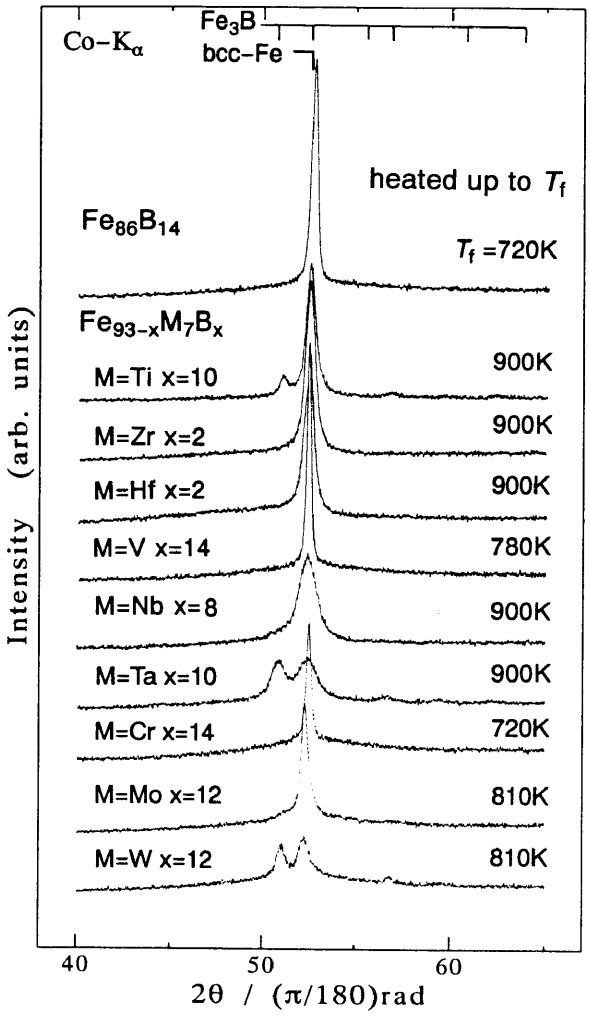

Fig. 4 X-ray diffraction patterns of amorphous $Fe_{93-x}M_7B_x$ (M=Ti, Zr, Hf, V, Nb, Ta, Cr, Mo and W) and $Fe_{86}B_{14}$ alloys heated up to T_f of 720, 780, 810 and 900 K at a constant heating rate of 0.17K/s.

Table I Final temperature of continuous heating (T_f), lattice spacing of $(110)_{bcc}$ plane (d_{110}), grain size of bcc phase (D), solubility at T_f (C_T) and solubility limit (C_a) of each M metal in α-Fe[12].

alloy	T_f / K	structure	d(110) / nm	D / nm	C_e (at%)	C_T(at%)
$Fe_{86}B_{14}$	720	bcc	0.2023	29	-	-
$Fe_{83}Ti_7B_{10}$	900	bcc+tetrag.	0.2029	19	10	≅1
$Fe_{91}Zr_7B_2$	900	bcc	0.2030	18	<1	<1
$Fe_{91}Hf_7B_2$	900	bcc	0.2029	19	<1	<1
$Fe_{79}V_7B_{14}$	780	bcc	0.2029	47	100	≅25
$Fe_{85}Nb_7B_8$	900	bcc	0.2028	10	<1	<1
$Fe_{83}Ta_7B_{10}$	900	bcc+tetrag.	0.203	≅10	<1	<1
$Fe_{79}Cr_7B_{14}$	720	bcc	0.2026	37	100	≅8
$Fe_{81}Mo_7B_{12}$	810	bcc	0.2035	27	25	≅2
$Fe_{81}W_7B_{12}$	810	bcc+tetrag.	0.203	≅15	14.3	<1

composed of the primary α-Fe and the B-enriched residual amorphous phases. This residual amorphous phase crystallizes to the tetragonal-Fe_3B compound at the second stage crystallization. The crystallization mechanism in amorphous $Fe_{92}Zr_8$ and $Fe_{91}Zr_7B_2$ alloys has previously been studied[11] and reported that these amorphous alloys follows primary crystallization. Since primary crystallization is controlled by long range atomic diffusion, its reaction speed becomes much slower than those for the polymorphous or eutectic crystallization which are controlled by interfacial diffusion. Polymorphous or eutectic crystallization are distinguished by their large reaction speed accompanying an exothermic peak which is sharper than that resulting from primary crystallization. Furthermore, the temperature interval in which the first exothermic reaction takes place in the DTA curves of other Fe-M-B alloys is nearly the same as those for the amorphous $Fe_{84}B_{14}$ or $Fe_{91}Zr_7B_2$ alloys. It is therefore presumed that the first stage exothermic reaction for all the other amorphous Fe-M-B alloys is also resulting from primary crystallization.

Table I summarizes the structure, grain size of the bcc phase and lattice spacing of $(110)_{bcc}$ plane (d_{110}) for the annealed Fe-M-B samples obtained by continuous heating up to T_f. The equilibrium solubility limit (C_e) and the solubility at T_f (C_T) of the M elements in α-Fe[12] is also shown in the table. The grain size was evaluated from the half-width of a $(110)_{bcc}$ diffraction peak. Although the grain size of the crystallization-induced phase in the Fe-M-B alloys containing V, Cr or Mo as a M element is in the range of 27 to 47 nm, the small grain size below 20 nm is obtained for the alloys containing Ti, Zr, Hf, Nb, Ta or W as a M element. The latter M elements are concluded to cause the formation of a nanocrystalline structure having a grain size below 20 nm. The M elements have a much lower solubility into α-Fe as compared with those for V, Cr and Mo, suggesting that the grain size of the primary bcc phase in the Fe-M-B systems is correlated with the

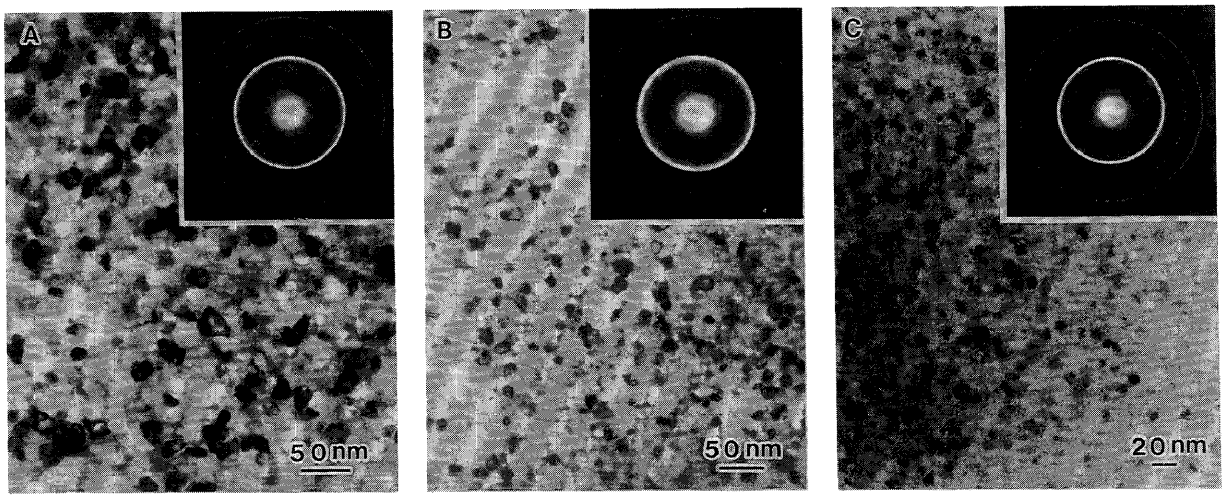

Fig. 5 Bright-field electron micrographs and selected area diffraction patterns of $Fe_{91}Zr_7B_2$ (a), $Fe_{91}Hf_7B_2$ (b) and $Fe_{84}Nb_7B_9$ (c) alloys annealed for 3.6 ks at 923K.

solubility limit of M elements in α-Fe. This assumption will be discussed in a later section. The formation of the nanocrystalline structure was also examined by TEM. The bright-field electron micrographs of the amorphous $Fe_{91}Zr_7B_2$, $Fe_{91}Hf_7B_2$ and $Fe_{84}Nb_7B_9$ alloys annealed for 3.6 ks at 923 K are shown in Fig. 5 (a), (b) and (c), respectively. The formation of the nanocrystalline structure with a grain size smaller than 20 nm is seen, being consistent with those evaluated from x-ray data.

3. 3. *Isothermal crystallization*

The kinetics of primary crystallization in the amorphous Fe-M-B alloys was studied by means of isothermal DSC measurements. An isothermal DSC trace at 758 K for an amorphous $Fe_{90}Zr_7B_3$ alloy is shown in Fig. 6. A bell-shaped exothermic peak, which corresponds to a nucleation-and-growth type transformation, is seen on the isothermal DSC trace of the amorphous Fe-Zr-B alloy. The fraction transformed (x) at time t of an isothermal nucleation-and-growth transformation can be described by the Johnson-Mehl-Avrami (JMA) equation (1);

$$x(t,t_i)=1-\exp[-k(t-t_i)n] \quad (1)$$

where t_i is the incubation time, k is a rate constant and n is the Avrami exponent which depends on the nucleation mechanism and growth morphology. The fraction transformed at 758 K was evaluated from the isothermal thermogram shown in Fig. 6. On annealing the sample at 723 K, no clear crystallization exotherm was detected on the isothermal thermogram because of its small reaction rate of the crystallization. Accordingly, the fraction transformed at 723 K was determined by measuring the annealing time dependence of the crystallization exotherm on the isochronal DSC trace for the samples which were annealed previously in a DSC cell at 723 K for different annealing times. Figure 7 shows plots of ln[-ln(1-x)] against ln(t-t_i) at annealing temperatures of 723 and 758 K for the amorphous $Fe_{90}Zr_7B_3$ alloy. The n value derived from the slope of each JMA plot within an x range of 0.2-0.8 shows the tendency to decrease with decreasing temperature, indicating that the nucleation mechanism and/or growth morphology of the primary bcc phase is a function of the annealing temperature. Because the amorphous $Fe_{90}Zr_7B_3$ alloy does not show the glass transition on its DSC trace at any heating rate in the present study, the crystallization of the amorphous $Fe_{90}Zr_7B_3$ alloy observed at 723 and 758 K is presumed to occur on a limited number of quenched-in nuclei** and steady-state nucleation during isothermal hold is negligible. Therefore, the increase of n with increasing annealing temperature is thought to reflect the increase of the dimensionality of crystal growth for the primary bcc phase, probably due to the change of the crystallization mode from surface- to bulk-crystallization. This result enable us to expect that the soft magnetic properties of the nanocrystalline Fe-M-B alloys are improved through the change of the morphology of the primary bcc precipitates by controlling the crystallization temperature.

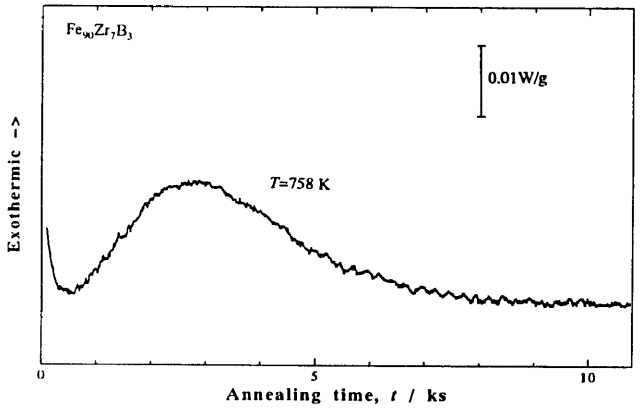

Fig. 6 Isothermal DSC trace for primary crystallization of nanocrystals in an $Fe_{90}Zr_7B_3$ alloy at 758 K.

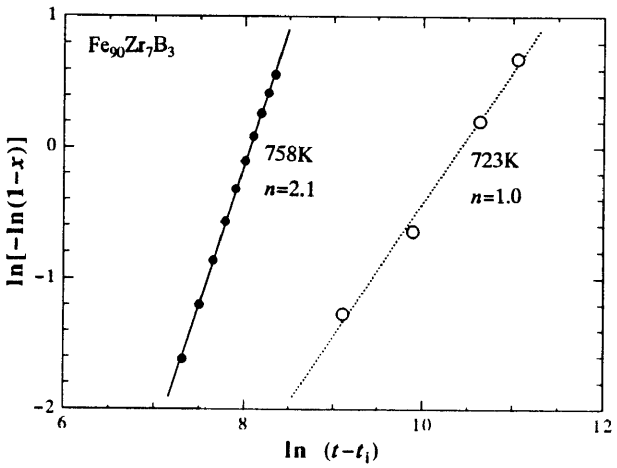

Fig. 7 JMA plot of DSC results for primary crystallization of nanocrystals in an $Fe_{90}Zr_7B_3$ alloy.

3. 4. *Influences of heating rate on nano-structure and soft magnetic properties*

Figure 8 shows bright- and dark-field electron micrographs of an amorphous $Fe_{90}Zr_7B_3$ alloy heated up to 923 K with a heating rate (α) of (a) 0.042 K/s and (b) 3.3 K/s, followed by isothermal annealing for 3.6 ks. The dark-field electron micrographs were taken from a part of the (110) reflection ring of the bcc phase. The grain size distribution of the annealed samples shown in Fig. 8(a) and (b) was evaluated by counting the bcc precipitates in each dark-field electron micrograph and is shown in Fig. 9(a) and (b), respectively. The grain size distribution of the bcc phase in the sample annealed at α=3.3 K/s is much narrower and the

**Köster and Herold have thought[10] that the quenched-in nuclei may not always possess the right structure and there may be some need for transformation taking some time until they become effective nuclei.

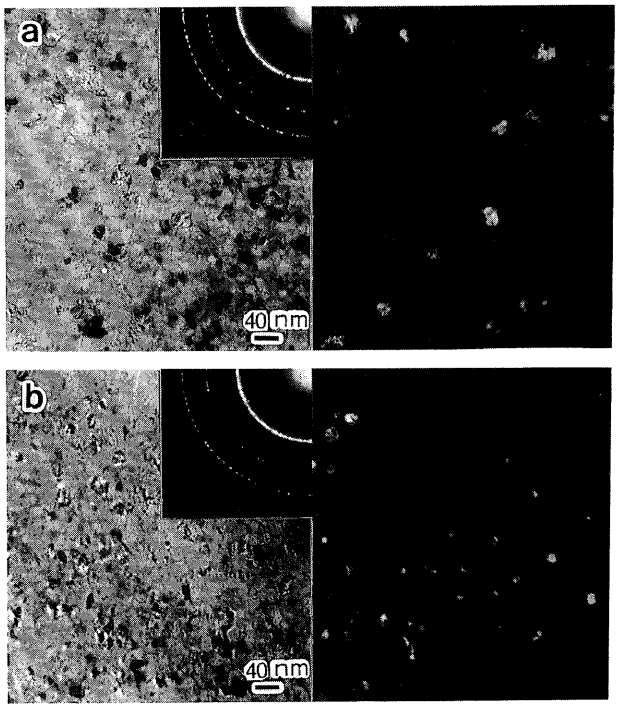

Fig. 8 Bright- and dark-field electron micrographs of an $Fe_{90}Zr_7B_3$ alloy annealed at 923 K for 3.6 ks with a heating rate (α) of 0.042 K/s (a) and 3.3 K/s (b).

mean grain size is much smaller, as compared with that in the one annealed at α=0.042 K/s. This decrease of the grain size with increasing α corresponds to an increase of the volume density of the primary bcc precipitates by a factor of about 3. Koster has carried out a systematic study on the influence of annealing temperature on the nucleation kinetics of amorphous alloys. In his study[10], it has been reported that the volume density of primary crystals tends to increase with the annealing temperature even below the glass transition. The onset temperature of the first-stage exothermic peak on the linear DSC trace for the amorphous $Fe_{90}Zr_7B_3$ alloy at α=0.042 K/s and 3.3 K/s was measured to be 777 K and 832 K, respectively. Therefore, the influence of heating rate on the microstructure is presumed to reflect the temperature dependence of the volume density of the primary bcc crystals.

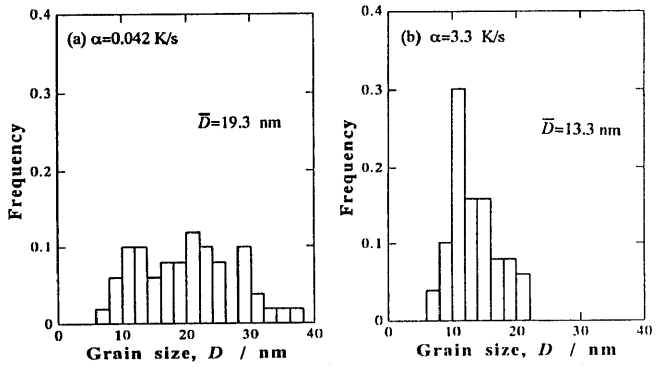

Fig. 9 Grain size distribution in an amorphous $Fe_{90}Zr_7B_3$ alloy annealed at 923 K for 3.6 ks with a heating rate (α) of 0.042 K/s (a) and 3.3 K/s (b).

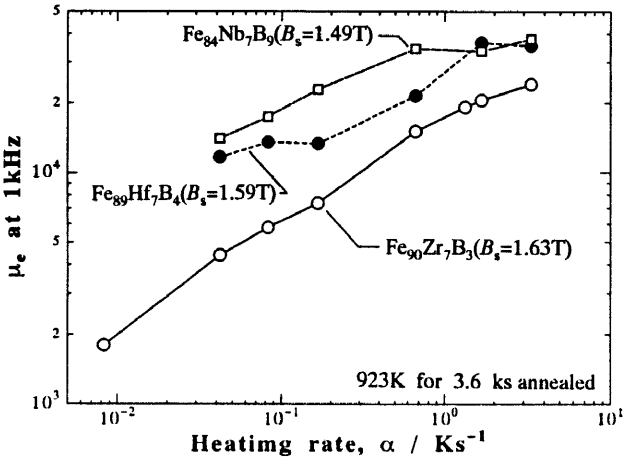

Fig. 10 Change in the μ_e value at 1 kHz and 0.4 A/m as a function of heating rate (α) for $Fe_{90}Zr_7B_3$, $Fe_{89}Hf_7B_4$ and $Fe_{84}Nb_7B_9$ alloys annealed for 3.6 ks at 923 K.

Figure 10 shows the change in relative permeability (μ_e) at 1 kHz and 0.4 A/m as a function of heating rate (α) for amorphous $Fe_{90}Zr_7B_3$, $Fe_{89}Hf_7B_4$ and $Fe_{84}Nb_7B_9$ alloys annealed for 3.6 ks at 923 K. The μ_e for all the Fe-M-B alloys shows the tendency to increase with increasing α. The magnetostriction of the $Fe_{90}Zr_7B_3$ alloy was measured to be as small as -1.1 x 10^{-6} to -1.6 x 10^{-6} within the α range of 0.083 to 3.3 K/s, showing that the significant increase of the permeability was due to the decrease of the apparent anisotropy resulting from the decrease of the grain size. Furthermore, the D value for the $Fe_{84}Nb_7B_9$ alloy at α=0.083 K/s and 3.3 K/s was evaluated to be 10.3 and 9.7, respectively, and thus the influence of α on the grain size of the primary bcc phase in the Fe-Nb-B alloy is much smaller, as compared with that in the Fe-Zr-B alloy. The difference in the gradient in each log-log curve shown in Fig. 10 can be explained by taking the difference of the influence of α on the grain size into the consideration.

3. 5. *Thermal stability of nanocrystalline structures*

The influence of annealing temperature on the grain size of the annealing-induced phase was examined for $Fe_{86}B_{14}$ and $Fe_{91}Zr_7B_2$ alloys. Figure 11 shows the change in the grain size of bcc phase (D) as a function of T_a, along with the data on the annealed structure determined by the x-ray diffractometry. The D value of $Fe_{86}B_{14}$ alloy is independent of T_a at temperatures below 673 K, however, it begins to increase with increasing T_a above 700 K where the annealing-induced phase changes to a mixed phase of α-Fe and Fe_3B. It should be noted that the grain coarsening of the bcc phase takes place accompanied by the phase change from bcc + B-enriched amorphous to α-Fe + Fe_3B and therefore, the reaction corresponding to the second exothermic peak in the DTA curve, shown in Fig. 3, appears to result the grain coarsening of the bcc phase. It is thought that the kinetics of grain coarsening is closely related to the grain boundary structure. In addition, the B-enriched amorphous

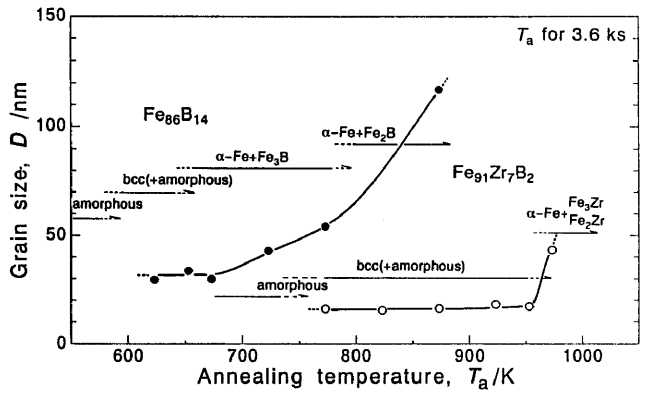

Fig. 11 Change in grain size (D) as a function of T_a for 3.6 ks for an amorphous $Fe_{91}Zr_7B_2$ alloy. The data of an amorphous $Fe_{86}B_{14}$ alloy are also shown for comparison.

phase, which remains in the grain boundary of the bcc phase, disappears by the crystallization at the second stage reaction. Therefore, it is reasonable to consider that the coarsening of the bcc grains is suppressed by the presence of B-enriched amorphous phase. And the increase of D observed in a T_a range above 700 K is presumed to result from the coarsening of the bcc grains induced by the disappearance of the B-enriched amorphous phase remaining in the grain boundaries. Similarly, the D values for $Fe_{91}Zr_7B_2$ alloy are independent of T_a in the range from 773 to 953 K by suppressing the grain coarsening resulting from the residual presence of the amorphous phase and further increase of T_a leads to the rapid increase of D, because the remaining amorphous phase starts to crystallize into compound phases. It has previously been reported[13] that the crystallization temperature of Fe-Zr-B amorphous alloys increases significantly with increasing solute content and a high crystallization temperature above 973 K is confirmed, being consistent with the present result that the amorphous phase enriched by solute elements remains in a T_a range up to 953 K. As described above, the grain coarsening of the nanocrystalline bcc phase is presumed to be dominated by the thermal stability of the amorphous phase remaining in the grain boundaries of bcc grains. It is ,thus, concluded that the precipitation of bcc phase due to the primary crystallization which brings about the enrichment of solute elements in the amorphous matrix, leading to the increase of its thermal stability, is essential for formation of nanocrystalline structure.

4. Discussion

4. 1. *Factors for formation of the nanoscale bcc structure*

As described in sections 2 and 3, the nanoscale bcc phase is formed by the primary crystallization of the amorphous phase with the nucleation due to the quenched-in nuclei. Here, we discuss the dominant factors for the formation of the nanoscale bcc phase on the basis of primary crystallization process. The formation of a primary crystalline phase with a small grain size is considered to be dominated by the following three factors; (1) crystallization due to a large number of nuclei, (2) crystallization with small growth rate, (3) high thermal stability of the resulting crystalline phase.

As shown in Fig. 1, relatively high μ_e values in all the Fe-M-B (M=Zr, Hf and Nb) alloys are obtained in the range along the boundary in which the phase field in a rapidly solidified state changes from an amorphous single phase to coexisting amorphous and bcc phases. It has further been confirmed[9] in the Fe-Hf-B system that the composition range in which the high μ_e values are obtained is in good agreement with that for the formation of the bcc structure with a small grain size less than 15 nm. The small grain size and the high μ_e values obtained for the Fe-M-B alloys are thought to originate from the formation of the amorphous phase with a high degree of the quenched-in fluctuation, presumably due to a relatively low glass-forming ability which may bring about a high transient nucleation rate during the solidification.

For primary crystallization of amorphous alloys, the growth rate of a primary crystalline phase has been thought to be controlled by volume diffusion. The radius (r) of growing precipitates by the diffusion control is expressed by equation (2);

$$r = K (D_c t)^{1/2} \quad (2)$$

here D_c is the diffusion coefficient and K is a dimensionless parameter. Accordingly, the small growth rate can be obtained by the small diffusivity and K. Figure 12 shows the compositional profiles which is expected for the growth process of primary nucleus in a simple binary system in a case that $r \cong \Delta r$, where C_o, $C_{(t)}$, C_b and C_a represent the compositions of an as-quenched amorphous phase, the amorphous matrix at time t, primary crystalline phase and the solute-enriched amorphous phase in equilibrium with the primary crystalline phase, respectively. The K value for this simple case is given by equation (3);

$$K = [2(C_a - C_{(t)})/(C_a - C_b)]^{1/2} \quad (3)$$

Accordingly, a small growth rate can be obtained by small D_c, C_b as well as large $C_{(t)}$. Although the actual compositional profile of growing precipitates in the present Fe-M-B is unknown and the calculation of the K value can not be made, this equation suggests that a small K value is expected when the solute element, which has the smallest diffusivity within the constituents, has a small solubility limit to the primary crystalline phase. This expectation is consistent with the result shown in Table I. That is, the grain size of the bcc phase which is smaller than that of the Fe-B binary alloy is obtained for the Fe-M-B alloys with the M elements having a small solubility limit less than 1 at%

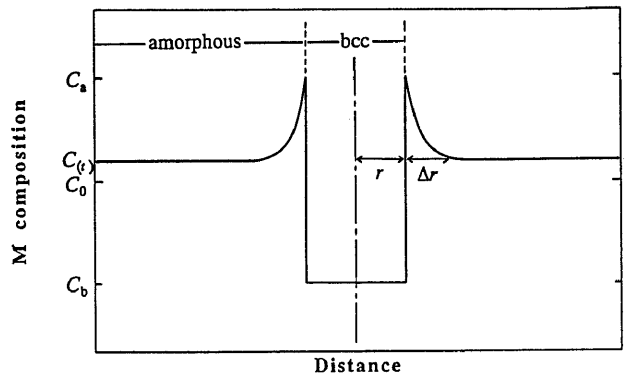

Fig. 12 Schematic view for composition profile expected through primary crystal.

in α-Fe and no refinement effect of the bcc grain is seen for the *M* elements having a large solubility limit exceeding the C_0 value (7 at%M).

After the primary crystallization reaction is completed, the grain coarsening of the primary crystals takes place. Therefore, the grain size of the bcc phase is dominate by the thermal stability of the residual amorphous phase which lies along the grain boundaries of the bcc phase. Since the remaining amorphous phase is thermally stabilized by the enrichment of *M* and B elements, the re-distribution tendency of *M* elements seems to be a dominant factor for the thermal stability of the remaining amorphous phase. In addition, the effect of additional transition elements on the thermal stability of Fe-metalloid amorphous alloys has been examined and it has been concluded[14] that the most stable amorphous phase are obtained in the alloy systems containing refractory metals with large atoms and low *d*-electron concentrations, particularly Zr, Hf, Nb and Ta. These previous data also support the present result that the formation of the nanocrystalline-bcc alloys with high thermal stability are obtained in the Fe-M-B (*M*=Zr, Hf and Nb) systems.

5. Conclusion

Crystallization behavior of the amorphous Fe-M-B (*M*=Ti, Zr, Hf, V, Nb, Ta, Cr, Mo and W) alloys and soft magnetic properties of annealing-induced alloys have been studied. The results are summarized as follows:

(1) The crystallization process of the amorphous Fe-M-B alloys can be classified into two types where the primary precipitates are a bcc single phase or coexistent bcc and tetragonal-Fe_3B phases. The former process was observed for amorphous Fe-M-B (*M*=Zr, Hf, V, Nb, Cr and Mo) alloys.

(2) The grain size of the primary bcc phase changed with the type of *M* elements and was evaluated to be 10 to 20 nm for *M*=Zr, Hf and Nb and larger values of 27 to 47 nm for V, Cr and Mo. Consequently, the formation of the mostly single bcc phase with a small grain size in the Fe-M-B ternary alloys is limited for Fe-M-B (*M*=Zr, Hf and Nb) systems. These *M* elements of Zr, Hf or Nb have a small solubility to α-Fe and the solubility limit is considerably smaller than those for V, Cr or Mo.

(3) The small grain size in the Fe-M-B (*M*=Zr,Hf and Nb) alloys seems to be attributed to the large re-distribution tendency of the *M* elements, which may cause a small growth rate of the primary precipitates, due to their small solubility to α-Fe.

(4) The volume density of primary bcc precipitates shows the tendency to increase with increasing heating rate. This microstructural change results in a significant increase of the permeability (μ_e) of the nanocrystalline alloys and a high μ_e value of 25000-38000 at 1 kHz and 0.4 A/m is obtained for the Fe-M-B (*M*=Zr, Hf and Nb) alloys annealed with a heating rate of 3.3 K/s.

(5) The grain size of annealing-induced bcc phase in $Fe_{91}Zr_7B_2$ alloy is almost independent of the annealing temperature while the metastable equilibrium of primary bcc and remaining amorphous phases is maintained. However, it changes significantly with annealing temperature when the compound phase begins to precipitate from the residual amorphous phase. This indicates that the thermal stability of the resulting nanocrystalline-bcc phase is dominated by that of the residual amorphous phase.

1) Y. Yoshizawa, S. Oguma and K. Yamauchi: J. Appl. Phys. 64 (1988) 6044 .
2) K. Suzuki, N. Kataoka, A. Inoue, A. Makino and T. Masumoto: Mater. Trans. JIM 31 (1990) 743.
3) Y. Fujii, H. Fujita, A. Seki and T. Tomida: J. Appl. Phys. 70 (1991) 6241.
4) G. Herzer: IEEE Trans. Magn. MAG-26 (1990) 1397.
5) K. Suzuki, A. Makino, A. Inoue and T. Masumoto: J. Appl. Phys. 74 (1993) 3316.
6) K. Hono, A. Hiraga, Q. Wang, A. Inoue and T. Sakurai: Acta Metall. 40 (1992) 2137.
7) U. Koster, U. Schunemann, M. Blank-Bewersdorff, S. Brauer, M. Sutton and G. B. Stephenson: Mater. Sci. Engn. A133 (1991) 611.
8) B. D. Cullity: *Elements of X-ray Diffraction 2nd ed. (Addison-Wesley, Reading, MA,* 1959) p. 262.
9) K. Suzuki, A. Makino, A. Inoue and T. Masumoto: J. Jpn. Inst. of Metals, 57 (1993) 964. [in Japanese]
10) U. Koster: *Proceedings on Phase Transitions '87, ed. G. W. Lorimer (The Institute of Metals, Cambridge* 1987) p. 597.
11) K. Suzuki, A. Makino, A. Inoue and T. Masumoto: Mater. Sci. Engn. A, to be published.
12) *Binary Alloy Phase Diagrams, ed. T. B. Massalski (ASM, Ohio,* 1986).
13) S. Ohnuma, M. Nose, K. Shirakawa and T. Masumoto: Sci. Rep. RITU, A29 (1981) 254.
14) I. W. Donald and H. A. Davies: Phil. Mag. A42 (1980) 277.